This document is downloaded from DR-NTU (https://dr.ntu.edu.sg)
Nanyang Technological University, Singapore.

Effect of TiO2 nanoparticle addition on electroless Ni–P under bump metallization for lead-free solder interconnection

Yang, Ying; Chen, Zhong; Hu, Xiao; Xu, Sha; Chan, Y. C.

2014

Hu, X., Xu, S., Yang, Y., Chen, Z., & Chan, Y. (2014). Effect of TiO2 nanoparticle addition on electroless Ni–P under bump metallization for lead-free solder interconnection. Materials Science and Engineering: A, 600, 67-75.

https://hdl.handle.net/10356/104454

https://doi.org/10.1016/j.msea.2014.02.011

© 2014 Elsevier B.V.This is the author created version of a work that has been peer reviewed and accepted for publication by Materials Science and Engineering: A, Elsevier B.V. It incorporates referee’s comments but changes resulting from the publishing process, such as copyediting, structural formatting, may not be reflected in this document. The published version is available at: http://dx.doi.org/10.1016/j.msea.2014.02.011

Downloaded on 23 Aug 2022 03:24:49 SGT

*Marked-up Manuscript

Effect of TiO_2 nanoparticle addition on electroless Ni-P under bump metallization for lead-free solder interconnection

Xiao HU[a], Sha XU[a], Ying Yang[b], Zhong Chen[b], Y. C. Chan[a,*],

[a]Department of Electronic Engineering, City University of Hong Kong,

Tat Chee Avenue, Kowloon Tong, Hong Kong

[b]School of Materials Science and Engineering, Nanyang Technological University,

Singapore 639798, Singapore

*Corresponding author. Tel.: +852 27887130; fax: +852 2788 7579.

E-mail address: eeycchan@cityu.edu.hk (Y.C. Chan).

Abstract

One primary purpose of this study is to introduce an electroless Ni–P–TiO_2 (17.5 at.% of P) composite coating as a pad finish for advanced electronic packaging. In this study, TiO_2 nanoparticles were incorporated into the Ni-P layer by electroless deposition and its function as novel under bump metallization (UBM) was intensively investigated. The majority of the added TiO_2 nanoparticles were proved to be uniformly distributed in UBM by scanning electronic microscopy (SEM) and X-ray diffraction (XRD). The interfacial reaction between electrolessly deposited Ni-P-TiO_2 layer and Sn-3.5Ag solder alloy was systematically analyzed. The prime Ni-P UBM was used for comparison to evaluate the effect of TiO_2 nanoparticle on the interfacial microstructure and mechanical property. Both solder/Ni-P and solder/Ni-P-TiO_2 joints were aged at temperature from 150°C to 190°C for different aging periods in order to study the intermetallic compounds (IMCs) growth and calculate the activation energy. It was found the growth of Ni_3Sn_4 IMC layer and void formation at the reaction interface were successfully suppressed with the help of the TiO_2 nanoparticle. The activation energies for the growth of Ni_3Sn_4 on Ni-

P and Ni-P-TiO_2 layer were calculated to be 50.9 kJ/mol and 55.7 kJ/mol, respectively. The extensive growth of Ni_3P and Ni-Sn-P phase as well as the consumption rate of the amorphous UBM was controlled in joints with TiO_2 nanoparticles. Thus Ni-P-TiO_2 UBM blocked the Cu diffusion from substrate to interface. A detailed reaction induced diffusion mechanism was proposed. The solder/Ni-P-TiO_2 solder joint consistently demonstrated higher shear strength than solder/Ni-P joint as a function of aging time. TiO_2 nanoparticle contributed to slow down the declining rate of shear strength from 0.021 Mpa/hour to 0.013 Mpa/hour with the aging time. Moreover, after the shear strength test, fracture mainly occurred at solder matrix of the solder/Ni-P-TiO_2 joint, the morphology showed a ductile fracture pattern with a large distribution of dimples on the rough surface.

Key words: lead-free solder, under bump metallization, electroless deposition, Ni-P-TiO_2, interfacial reaction, shear strength

1. Introduction

Due to the ever increasing environment concern, lead free soldering is the irreversible trend in microelectronic packaging. On the other hand, fine-pitch in the electronic device called for the scale down of the semiconductor component. The miniaturization brings great challenge to the solder interconnect. Both the increased melting point of lead free solder alloy and the decreased joint dimension have exacerbation of the interfacial reaction. The morphology and growth of IMCs at interface is essential for determining the mechanical reliability of the interconnect. Electroless Ni-P has been recognized to be better than copper substrate during soldering due to its better barrier property. The characteristics of low cost, good solderability and uniform thickness make electroless Ni-P a constant focus in both industry and academia for years [1-5]. During the soldering process, Ni_3Sn_4 is the primary IMC. However, the solder-reaction assisted crystallization is simultaneously happened at interface.The formation of P-rich layer and ternary Ni-Sn-P alloy underneath Ni_3Sn_4 by Ni atoms diffusion may lead to the formation of voids, or even make the interface prone to cracks finally [6,7]. Moreover, ternary Ni-Sn-P alloy induced IMC spallation from UBM layer is another threat to severe degradation of the solder joint reliability [8].

To improve the solder interconnect reliability, many researchers focus their attention on the solder matrix. Both metallic and nonmetallic materials have been added into the solder matrix by various methods to reinforce the joint, such as mechanical stirring solder paste, mixing the solder powder and sintering [9-12]. UBM and solder alloy are equally important for good interconnect. However, fewer researchers concentrated on the UBM modification to reinforce the solder joint. Yang et al. have added third element, tungsten in Ni-P layer; and this Ni-P-W UBM significantly retarded interfacial reaction with lead-free Sn–3.5Ag solder [13]. Carbon nanotube has been used by Gu's group to deposit Ni-P-CNT composite coating, the result showed it successfully slowed down the growth rate of Ni_3Sn_4 IMC layer and the P rich layer [14]. Ni-Sn-P UBM has been used by Yang et al. to suppress the void formation during soldering [15]. Furthermore, Sohn et al. have changed the P content in Ni-P UBM, and found its close relationship with IMC spallation [8].

TiO_2 has been used to improve the corrosion resistance of the composite coating [16]. Asit et al. has doped 1 wt% TiO_2 nanoparticle in Sn–Ag–Cu solder matrix, resulting in a finer microstructure and suppressed IMC growth [17]. From literature, TiO_2 nanoparticle is seldom used in UBM for electronic packaging. In this work, TiO_2 nanoparticles have been successfully added to the Ni-P layer (17.5 at.% of P) to form Ni-P-TiO_2 composite by electroless deposition. Both Ni-P and Ni-P-TiO_2 were reacted with Sn-3.5Ag solder to form solder joint. The atom diffusion induced interfacial reaction and microstructure evolution of the joints were systematically investigated after different aging condition. The growth kinetics and activation energies of IMC formation were calculated. The effect of TiO_2 on interface was highlighted with comparison. Moreover, the shear test was conducted to evaluate the mechanical property of solder/Ni-P-TiO_2 joint.

2. Experimental

Titanium dioxide nanoparticles with dimension of 21 nm were bought from Evonik degussa. Cu foils (5 mm thick, 99.97 wt.%) were used as the substrate for both Ni–P and Ni-P-TiO_2 plating. Prior to both plating, the Cu substrates were polished and etched with 30 vol.% nitric acid for 30 s, followed by a

commercial Pd activation treatment (planar preinitiator solution from MacDermid) for surface activation. The Ni-P-TiO_2 plating bath was prepared by disperse TiO_2 nanoparticles into the commercial Ni-P plating bath (from MacDermid). The TiO_2 nanoparticle with an amount of 3g/L in solution was first ultrasonic processed for 1 hour to avoid agglomeration, followed by magnetic stirring at 500 rpm for 40 minutes to ensure a uniform dispersion of TiO_2 nanoparticles in the Ni–P plating bath. The concentration of TiO_2 nanoparticle in plating solution was optimized by previous experiment. The commercial Ni–P plating bath without TiO_2 nanoparticle was used for prime Ni-P layer (17.5 at.% of P) deposition as comparison. The pH levels of plating solution were adjusted to be 5.3 by ammonia hydroxide. Both the electroless plating processes were conducted at 84±1 ℃ for 30 min.

Then both deposited layers were tested by a thin film X-ray diffractometer (XRD) with Cu K α source (Shimadzu XRD 6000) for phase identification. The surface morphology of the Ni-P and Ni-P-TiO_2 layers was observed by atomic force microscope (AFM, Veeco, Santa Barbara, CA) and scanning electron microscope (SEM, Philips XL 40 FEG). Sn-3.5Ag solder ball with rosin mildly activated (RMA) flux was used to form solder joint with Ni-P and Ni-P-TiO_2 layer. The soldering process was carried out in an 8-zone forced convection reflow oven (BTU Pyramax 100N, North Billerica, MA). The reflow profile was set with a peak temperature of 250 °C; and the time above the melting temperature of the Sn-3.5Ag solder was about 70 seconds, the reflow profile is shown in Fig.1.

For the interfacial microstructure characterization, the samples were mounted in resin and cross sectioned by carefully grinding towards the center using sand paper of different grit sizes followed by polishing with 0.5 μm alumina suspension. Finally, the solder/UBM interfacial microstructure was observed using SEM under back-scattered electron (BSE) imaging mode. An energy dispersive X-ray spectrometer (EDX, International, Model No. DX-4) was utilized to perform the semi-quantitative analysis on the microstructures to determine the chemical composition and the phase. Leica LAS V3.8 image process software was used to measure the average thickness, which was obtained through dividing the measured area by the horizontal length.

To measure the shear strength, ball shear tests were performed on samples after aging for different time spans using a shear testing machine (DAGE Series 4000 Bond tester, UK) with a test speed of 350 μm/s. The diameter of the contact interface was 0.17 mm^2. The fracture surfaces and compositions were investigated thoroughly using SEM under secondary electron (SE) imaging mode. Shear stress testing of 30 solder balls was undertaken at each condition, with the minimum and maximum values removed.

3. Results and Discussion

The electrolessly deposited Ni-P and Ni-P-TiO_2 UBM is shown in Fig.2. The morphology of the Ni-P layer has slight protuberances with different dimensions in a close-packed structure (Fig.2(a)). In Fig.2(c), the TiO_2 nanoparticles were distinctly observed on the surface of the deposited Ni-P-TiO_2 layer. Despite the slight agglomeration, the TiO_2 nanoparticles were uniformly distributed over the whole UBM surface. The size of protuberances in Ni-P-TiO_2 was not as even as that in Ni-P layer. The average thickness of the Ni-P and Ni-P-TiO_2 were 7.1 μm and 7.6 μm, respectively. No voids were detected between UBM and Cu substrate in both samples, indicating a good adhesion between both types of coatings and substrate. Both kinds of UBM has 17.5±1 at.% of P according to the EDX.

As shown in Fig.3, the X-ray diffraction pattern of both Ni–P and Ni-P-TiO_2 coatings in their as-prepared state demonstrated a broad peak centered 2θ at around 45°, referring to Ni (1,1,1) phase, indicating both layers have an amorphous structure. It's well consistent with G. Dietz's result that Ni-P layers with about 12–20 at.% P were found to be amorphous [18]. However, a distinct TiO_2 peak was detected at around 25° in Ni-P-TiO_2. This finding further confirmed the existence of TiO_2 nanoparticles which were embedded in the UBM with a uniform distribution.

AFM images of Ni-P and Ni-P-TiO_2 are shown in Fig.4. The root mean square roughness observed in plain Ni-P and TiO_2 doped Ni-Players were 173 and 245 nm, respectively.The nodules-like surface morphology of Ni-P-TiO_2 coating, may be attributed to incorporation of TiO_2 nanoparticles. It is revealed that with the TiO_2 nanoparticles addition, the doped Ni-P layer shows a much bumpier morphology than the plain Ni-P layer.

Fig.5 shows the cross-section microstructure at as-reflowed Sn-3.5Ag/Ni-P and Sn-3.5Ag/Ni-P-TiO_2 joints interface. EDX result showed the primary IMC of Sn-3.5Ag/Ni-P joint was conventional Ni_3Sn_4 phase. The formation of Ni_3Sn_4 resulted from reaction between Ni atoms diffused from Ni-P layer and Sn atoms diffused from solder. This IMC layer had a scallop shape with average thickness of 2.09 μm (Fig.5(a)). Another kind of IMC Ag_3Sn was detected near the interface, but the quantity was small due to the low percentage of Ag in the solder alloy. The formation of the Ni_3Sn_4 in Sn-3.5Ag/Ni-P-TiO_2 joint is shown in Fig.5(b). The small rod like Ni_3Sn_4 IMC layer closely adhered to the uneven Ni-P-TiO_2 UBM layer. Spallation of the Ni_3Sn_4 phase into the solder matrix was hardly observed in both plain and TiO_2 doped samples. A very thin layer of Ni_3P was present between Ni_3Sn_4 and Ni-P metallization, but it is difficult to detect Ni_3P layer adjacent to Ni-P-TiO_2 metallization.

Fig.6 shows the solder/Ni-P and solder/Ni-P-TiO_2 joints after aging at 150°C for 100 hours. The thickness of Ni_3Sn_4 layer increased compared to the as-reflowed samples. The TiO_2 incorporated sample showed a smaller thickness compared to the plain sample. The shape of Ni_3Sn_4 IMC formed in both samples transformed to chunky-type. Small part of the Ni-P layer (about 0.82 μm) has transformed into Ni_3P phase with 15.5±1 wt.%P and 74.5±1 wt.%Ni in Sn-3.5Ag/Ni-P joint. The formation of Ni_3P is a result of out-diffusion of Ni atoms from Ni-P layer to react with Sn. This process assisted the amorphous Ni-P layer partially transform into crystalline Ni_3P phase. At the interface, Sn and Ni atoms had different diffusion rate. The Ni-P layer continued to provide Ni atoms to react with Sn, while no other atoms can compensate the lattice vacancy left by the Ni atoms in Ni_3P layer. As a result, kirkendall voids were present perpendicularly to Ni_3P layer between solder and Ni-P layer formed at the solder/Ni-P interface as shown in Fig.6(a). It is noteworthy that there were no kirkendall voids appeared at the solder/Ni-P-TiO_2 joint interface (Fig.6(b)). The upper side of the Ni_3Sn_4 layer was in flash burr shape, indicating part of this IMCphase has not yet thoroughly changed from small rod-type to chunky-type.

Fig.7 shows the microstructure of both kinds of reaction couples after aging at 200°C for 625 hours. The Ni_3Sn_4 IMC kept growing as the aging continues. With the same aging condition, the thickness of Ni_3Sn_4

in solder/Ni-P-TiO_2 joint was 8.21 μm (Fig.7(b)), which was 3.19 μm thinner than that formed in solder/Ni-P joint (Fig.7(a)). The difference in thickness under the same aging condition proved TiO_2 had helped retard the Ni_3Sn_4 IMC layer growth. The addition of TiO_2 nanoparticles as the second phase contributed to alter the diffusion rate and driving force of Ni_3Sn_4 phase growth. According to Li et al. [19], the third element added in the reinforced solder alloy helped to reduce the IMC growth by changing the thermodynamic parameters of elemental affinity and the diffusion coefficient. In the present study, TiO_2 nanoparticles acted as the similar way on the metallization to reinforce the solder joint. As TiO_2 nanoparticle is a non-reactive, non-coarsening material, it maybe adsorbed at the grain boundary, thus the relative relationship of the growth rates among the crystal orientations of the Ni_3Sn_4 phase are changed, leading to a suppression of the Ni_3Sn_4 layer growth. In solder/Ni-P joint, after aging at 200 °C for 625 hours, the thickness of the crystalline Ni_3P layer expanded to 4.42 μm, which was more than three quarters of the initial thickness of the amorphous Ni-P UBM. On the contrary, Ni_3P layer in TiO_2 doped joint was still very thin and voids can hardly be detected in this layer. Many researchers reported the existence of nanocrystalline Ni-Sn-P layer between Ni_3Sn_4 layer and Ni_3P layer in the case of Ni-P UBM, which was the main cause for IMC spalling [3]. In the present study, a very thin layer of Ni-Sn-P was detected adjacent to the Ni_3P layer. A detailed study on this ternary Ni-Sn-P phase will be conducted in future by TEM. In the solder/Ni-P joint, another Cu containing phase was formed with an irregular cluster appearance and gradually expanded towards the thick Ni_3Sn_4 layer. EDX result showed this phase contains 20.5±1 wt.% Ni, 5.5±1 wt.% Cu and 74±1 wt.% Sn, suggestive of $(Ni_{1-x}Cu_x)_3Sn_4$ phase. The formation of $(Ni_{1-x}Cu_x)_3Sn_4$ phase indicated the Cu atoms managed to diffuse from Cu substrate through thin Ni-P and thick Ni_3P layer to incorporate into IMC formation. Ni-P layer has an amorphous structure which is difficult for copper to diffuse through. However, columnar grains of Ni_3P layer act as a good channel for Cu diffusion. As the reaction proceeded, crystalline Ni_3P layer grew thicker at the expense of the amorphous Ni-P layer. When most of the Ni-P layer was transformed into the crystalline Ni_3P layer, it would be much easier for Cu atoms to diffuse through the Ni-P and Ni_3P layers, resulting in the formation

of $(Ni_{1-x}Cu_x)_3Sn_4$ phase. In the solder/Ni-P-TiO_2 joint, due to the barrier property of TiO_2 nanoparticle, the growth of Ni_3P and Ni-Sn-P phases was quite slow and the interface between the solder and metallization remained uneven. TiO_2 successfully reduced the diffusion of Ni atoms thus decreased the consumption rate of the amorphous Ni-P layer. In solder/Ni-P-TiO_2 joint, after prolonged aging, only a small amount of amorphous UBM layer transformed into crystalline Ni_3P layer, so it was difficult for Cu to penetrate through the UBM and IMC layer with few grain boundaries to the interface.

In general, the growth of the intermetallic layer is dominated by the volume diffusion. The IMC growth process can be described by a typical parabolic equation [20, 21] given below:

$$x - x_0 = k^{0.5} t^{0.5} \quad (1)$$

Where x is the thickness of the Ni_3Sn_4 layer at t time, x_0 is the initial Ni_3Sn_4 layer thickness at the as-reflowed state, t is the aging time, k is the growth rate constant (cm^2/s) which is also regarded as the diffusion coefficient of elements in IMC layer.

Solder/Ni-P and solder/Ni-P-TiO_2 joints were aged at 150℃, 170℃ and 190℃ for different period. Fig.8 demonstrates the average IMC layer thickness increment (x-x_0) for solder/Ni-P and solder/Ni-P-TiO_2 joints versus the square root of aging time. From the graph, the average Ni_3Sn_4 layer thickness is proportional to the square root of aging time, and the value of k is determined from the slope of the linear regression line. The estimated k value of Ni_3Sn_4 in two kinds of joints are listed in table 1, the growth rate constant increased as the temperature grow from 150°C to 190°C, implying the Ni_3Sn_4 layer grows faster at high temperature. He et al. has calculated the diffusivity k to be 1.12×10^{-14} cm^2/s at 150°C, 2.49×10^{-14} cm^2/s at 170°C and 7.7×10^{-14} cm^2/s at 190°C, respectively [22]. Their result is relatively smaller than the diffusivity obtained in the present solder/Ni-P joint. It may ascribe to different method of soldering-reflow and volume of the liquid phase in particular [13], moreover dimension of contact area between solder and UBM may also contribute to the difference in growth rate constant. Due to the barrier function of TiO_2 nanoparticles doped in the metallization, the growth rate constant of the IMC layer is reduced by more than

half from its value in the case of plain UBM for all the three temperature points, under the same experimental condition as shown in table 1.

The Arrhenius relationship is also applicable as below

$$k = k_0 \exp\left(-\frac{Q}{RT}\right) \qquad (2)$$

Where k_0 is the constant growth rate (cm^2/s), Q is activation energy for IMC growth (kJ/mol), R is ideal gas constant (8.314 J/mol K) and T is absolute temperature (Kelvin). The value of Q can be deduced from the slope of the Arrhenius plot as shown in Fig.9. The activation energy of the Ni_3Sn_4 growth in the aging condition were calculated to be 50.9 kJ/mol for solder/Ni-P joint and 55.7 kJ/mol for solder/Ni-P-TiO_2 joint, respectively. The solder with the TiO_2 doped UBM showed a smaller Q value, indicating more energy was needed for the Ni_3Sn_4 layer growth. Jeong-Won Yoon et al. reported the activation energy of Ni_3Sn_4 in Sn–3.5Ag/Ni–P/Cu system to be 49 kJ/mol at temperatures from 100℃-170℃ for up to 60 days [4]. Chang-Bae Lee et al. calculated the Q value in Sn-3.5Ag/Au/Ni-P joint to be 72.5 kJ/mol, and the aging condition was from 70℃-170℃ for as long as 60 days [23]. Despite some difference in experimental conditions, the estimated Q value in present work is in the acceptable range when compared with the previous work. Therefore, it proves Sn diffusion in Ni_3Sn_4 still act as the controlling mechanism for IMC growth similar to the previous work. The TiO_2 nanoparticles exist in the Ni-P layer; they successfully hinder the out-diffusion of Sn atoms from solder matrix towards the metallization thus lead to limited supply of Sn atoms for interfacial reaction, resulting in profound obstacle to form Ni_3Sn_4 phase.

Fig.10 shows a magnified IMC image from solder/Ni-P joints aged at 200℃ for 750 hours. It shows the UBM has fully transformed to crystalline Ni_3P phase. The Cu diffusion induced $(Ni_{1-x}Cu_x)_3Sn_4$ phase grew dramatically and expanded to a considerable portion of Ni_3Sn_4 layer. Some cracks can be observed inside the $(Ni_{1-x}Cu_x)_3Sn_4$ phase. Volume change in $(Ni_{1-x}Cu_x)_3Sn_4$ phase generated stress, resulting in void formation at the interface between $(Ni_{1-x}Cu_x)_3Sn_4$ phase and Ni_3Sn_4 phase. The voids would nucleate and propagate with increasing aging time, and then gradually expanded to initiate cracks.

Fig.11 shows the schematic mechanism of solder/Ni-P and solder/Ni-P-TiO_2 interfacial reaction. Ni concentration difference drives Ni atoms diffuse from UBM to the solder matrix. The Sn atoms from solder matrix are also driven by the concentration difference to react with Ni to form Ni_3Sn_4 IMC layer. In Fig.11(b), the TiO_2 nanoparticles appeared on the Ni-P layer, blocked the diffusion path of Sn and Ni atoms to interface, and resulting in the decreased Ni_3Sn_4 layer thickness. In the plain Ni-P joint, due to the fast formation of Ni_3Sn_4 layer, Ni atoms become significantly depleted in the UBM. This process assisted the transformation of amorphous Ni-P layer into crystalline Ni_3P phase. According to Liu et al. [24], structure of Ni_3P phase has many very fine grains, which act as fast diffusion channel and enhance the diffusion of Ni to penetrate the Ni_3P to solder matrix. Due to the doping of TiO_2 nanoparticle, the reaction-assisted process is alleviated to some extent as the atoms movement is restricted, resulting in formation of less crystalline Ni_3P phase and few voids formed at interface in Fig.11(b). In sample without TiO_2 nanoparticle, Ni atoms are consumed from electroless Ni-P through grain boundaries of Ni_3P layer to form Ni_3Sn_4 phase. This out-diffusion of Ni atoms triggered counter diffusion of vacancies. Not enough atoms are able to compensate the lattice vacancy left by the Ni atoms in Ni_3P layer, so columnar voids are formed in Ni_3P layer perpendicularly of as shown in Fig.11(a). As the reaction proceeded, Sn atoms from solder matrix will react with nickel from upper part of crystalline Ni_3P layer to form Ni-Sn-P phase though a complicated reaction process [7]. In Fig.11(a), when the crystalline Ni_3P layer keep growing to occupied majority area of the UBM, Cu atoms from the substrate managed to diffuse through the fine grains of Ni_3P layer to react with Ni and Sn atoms to form irregular cluster shaped $(Ni_{1-x}Cu_x)_3Sn_4$ phase. The presence of Kirkendall voids in Ni_3P layer also facilitate the of Cu diffusion to trigger the dramatically expansion of $(Ni_{1-x}Cu_x)_3Sn_4$ phase in Ni_3Sn_4 layer. The irregular shape of $(Ni_{1-x}Cu_x)_3Sn_4$ phase may be ascribed to the different size and quantity of voids in Ni_3P layer. These voids acted as the dominant diffusion channel for Cu atoms to penetrate through. With the effect of TiO_2 nanoparticle, Ni atom diffusion from UBM towards solder is obstructed. So enough Ni atoms stay in the UBM to inhibit the growth of crystalline Ni_3P. TiO_2 nanoparticles act as a barrier to slow down the unbalanced inter-diffusion between Sn and Ni at the

Ni_3Sn_4/solder interface, thereby further retard the interfacial reaction and avoid significant shrinkage of amorphous Ni–P-TiO_2 layer. As Cu is very difficult to penetrate the amorphous structure, the formation of $(Ni_{1-x}Cu_x)_3Sn_4$ phase is suppressed as shown in Fig.11(b). Volume mismatch induced by transformation between Ni_3Sn_4 and $(Ni_{1-x}Cu_x)_3Sn_4$ phase result in a local boost of huge amounts of stress inside the IMC. Such a high local stress will create physical voids [25-27]. As reaction proceeds, the voids propagate to form cracks and expand in $(Ni_{1-x}Cu_x)_3Sn_4$ phase as shown in Fig.10. The cracks in the IMC are possible to induce catastrophic failure of interconnect. Moreover, this newly formed phase is unable to play a mechanical interlocking role at the interface between solders and metallization, thus severely threats the reliability of the solder joint. In this way, TiO_2 nanoparticle addition is able to improve the reliability of the interconnect by decreasing of IMC layer thickness while inhibit the voids and cracks formation under circumstances of aging.

Shear strength is an essential mechanical property regarding to the reliability of solder joint. Solder interconnect often encounters external mechanical loading during processing as well as service, thus superior shear strength promises a better reliability for the electronic system. Ball shear tests were conducted to evaluate the effect of the TiO_2 nanoparticle on the mechanical properties of the modified Sn-3.5Ag/Ni-P solder joints as a function of aging time. Fig.12 demonstrates the assessment of the average shear strength of solder/Ni-P and solder/Ni-P-TiO_2 joint aged for different durations. For both kinds of joint, the shear strength decreased as the aging continued. The as-reflowed solder/Ni-P-TiO_2 joint had the highest shear strength of 43.2 MPa which is 1.9 MPa higher than that of the as-reflowed solder/Ni-P joint. Throughout the aging periods, solder/Ni-P-TiO_2 joint maintains higher shear strength than the plain sample despite the decline. The shear strength of solder/Ni-P joint declined at a rate 0.021 Mpa/hour at 190℃ for 625 hours. The strength of solder/Ni-P joint reduced to 32.2% by the end of the aging period. In contrast, the decline rate decreased to be 0.013 Mpa/hour in solder/Ni-P-TiO_2 joint. The strength reduced by only 19.0% by the end of the aging period. The better reliability of solder/Ni-P-TiO_2 joint under shear test upon aging attributes to TiO_2 nanoparticle reinforcement. According to a dispersion strengthening mechanism

[28], the homogeneous distribution of TiO_2 nanoparticle on the UBM together with the well-controlled thickness of IMC layer contributes to the improvement of mechanical property. They not only help suppress the grain boundaries from sliding, but also increase dislocation densities and retard the dislocations movement. Compared with the UBM without TiO_2 nanoparticles, the rough and uneven morphology of the electroless deposited Ni-P-TiO_2 layer is prone to form a stable and ductile bonding with the solder thus perform better to defend external mechanical loadings.

After the shear test, the fractographic analyses of the solder/Ni-P and solder/Ni-P-TiO_2 joints were carried out by SEM to investigate the root cause for degradation of the shear strength. The SEM images of the fracture surface for both kinds of joints aged at 190℃ are shown in Fig.13 for detailed analysis. In the joint without TiO_2 nanoparticle aged for 400 hours, part of the bulk solder was removed by the shear blade and an underneath layer was exposed. This exposed layer was identified to be a mixture of IMCs and Ni-P UBM. The remained solder fracture surface showed a brittle fracture pattern with a quite smooth morphology. As shown in Fig.13(b), after aging for 625 hours, majority of the solder matrix was stripped off and less solder alloy remained on the fracture surface, so it can be confirmed that fracture happened mainly on the interface rather than solder matrix after prolonged aging time. Sohn et al. have reported brittle fracture usually occurred between the Ni_3Sn_4 IMC and the Ni-P layer [29]. However, the fracture occurred in solder/Ni-P-TiO_2 joints was mainly through solder matrix even when the aging time is as long as 625 hours. The fracture surface exhibited a ductile transition appearance, with many dimples and plastic deformation observed on the tensile plastic fracture. It is attributed to the homogeneous distribution of the TiO_2 nanoparticle on the Ni-P layer. The residual Sn-3.5Ag solder indicates that the fracture path was inside the solder matrix which proved the bonding stress of IMCs was stronger than the cohesive of solder matrix after aging for 625 hours. In contrast, for the solder/Ni-P joint, the fracture path shifted from inside to the bulk solder to interface after aging for 625 h. This is because the thick Ni_3Sn_4 layer in solder/Ni-P joint may exceed the critical value, leading to a weaker interface bonding than the bulk solder [6]. In solder/Ni-P joint, excessive growth of the intrinsically brittle Ni_3P and Ni-Sn-P layers with voids and

cracks at interface without TiO_2 nanoparticles could easily provide a path for brittle fracture [30-32], thus severely deteriorate joint the mechanical property. In contrast, the less significant porosity in the solder/Ni-P-TiO_2 joint interface due to TiO_2 nanoparticle addition evidently assists to boost the shear strength. Chan et al. reported the brittle fracture pattern was a premonition which most likely to cause severe failure of interconnect [33]. Therefore, TiO_2 reinforced UBM helps to reinforce the shear strength of solder joint, thus improve the reliability of the interconnect.

4. Conclusion

In the present work, novel Ni-P-TiO_2 composite layer was electrolessly deposited as UBM for lead-free soldering in electronic packaging. SEM observation and XRD results prove that the TiO_2 nanoparticles were uniformly distributed in UBM. The interfacial reaction induced microstructural evolution between solder and Ni-P-TiO_2 layer was systematically analyzed and prime Ni-P layer was used as comparison. Both solder/Ni-P and solder/Ni-P-TiO_2 joints were aged at different temperatures for various aging periods in order to study the IMC growth kinetics and calculate the activation energy. It was found that the growth of Ni_3Sn_4 IMC layer and void formation at interface were greatly retarded with the help of the TiO_2 nanoparticle. The activation energies for the growth of Ni_3Sn_4 on Ni-P and Ni-P-TiO_2 layer are calculated to be 50.9 kJ/mol and 55.7 kJ/mol, respectively. The growth of Ni_3P and Ni-Sn-P layers as well as the consumption of the amorphous UBM is suppressed by addition of TiO_2 nanoparticle in UBM. Thus the Cu diffusion from substrate to interface is hindered in Ni-P-TiO_2 UBM. The reaction induced diffusion mechanism was intensively investigated. The solder/Ni-P-TiO_2 solder joint consistently demonstrated higher shear strength than solder/Ni-P joint as a function of aging time. TiO_2 nanoparticle contributes to slow down the declining rate of shear strength with aging from 0.021 Mpa/hour to 0.013 Mpa/hour. Moreover, fracture mainly occurred at solder matrix of the aged solder/Ni-P-TiO_2 joint after the shear strength test, the morphology showed a ductile fracture pattern with a large distribution of dimples on the rough surface. In summary, the Ni-P-TiO_2 composite layer is shown to be a promising alternative UBM with barrier property for advanced electronic packaging.

Acknowledgments

The authors would like to acknowledge the financial support provided by the Research Grants Council, Hong Kong, Ref. no. 9041636 (A study of nanostructured electronic interconnects-preparation, characterization and integration), City University of Hong Kong Research project: 7002848 (A study of functionalized CNT/graphene reinforced composite electronic interconnects: preparation, characterization and integration for green nanoelectronic applications), the Centre for Electronic Packaging & Assemblies, Failure Analysis & Reliability Engineering (EPA Centre) of City University of Hong Kong and School of Materials Science & Engineering, Nanyang Technological University for hosting Hu Xiao as research exchange student in 2013.

References

[1] M. He, W.H. Lau, G.J. Qi and Z. Chen, Thin Solid Films. 462 (2004) 376–383.
[2] D. M. Jang and J. Yu, J. Mater. Res. 26 (2011) 889-895.
[3] Y.C. Lin, K.J. Wang and J.G. Duh, J. Electron. Mater.39 (2010) 283-294.
[4] C.F. Tseng, C. J. Lee and J.G. Duh, Mater. Sci. Eng. A-Struct. Mater. Prop. Microstruct. Process. 574(2013) 60-67.
[5] C.F. Tseng and J.G. Duh, Mater. Sci. Eng. A-Struct. Mater. Prop. Microstruct. Process. 580(2013) 169-174.
[6] M. He, Z. Chen and G. Qi, Metall. Mater. Trans. A. 36 (2005) 65–75.
[7] Y.C. Lin, T.Y. Shih, S.K. Tien and J.G. Duh, Scripta. Mater. 56 (2007) 49–52.
[8] Y. Sohn, J. Yu, S. Kang, D. Shih and T. Lee, J. Mater. Res. 19 (2004) 2428–2436.
[9] X. Hu, Y.C. Chan, K. Zhang, and K. Yung, J. Alloys Compd. 580 (2013) 162-171.
[10] C.L. Chuang, L.C. Tsao, H.K. Lin and L.P. Feng, Mater. Sci. Eng. A-Struct. Mater. Prop. Microstruct. Process. 558(2012) 478-484.
[11] A.A. El-Daly, A. Fawzy, S.F. Mansoura and M.J. Younis, Mater. Sci. Eng. A-Struct. Mater. Prop. Microstruct. Process. 578(2013) 62-71.
[12] Z.B. Yang, W. Zhou and P. Wu, Mater. Sci. Eng. A-Struct. Mater. Prop. Microstruct. Process. 590(2014) 295-300.
[13] Y. Yang, J.N. Balaraju, S.C. Chong, H. Xu, C.Q. Liu, V.V. Silberschmidt and Z. Chen, J. Alloys Compd. 565 (2013) 11–16.
[14] X. Gu, Y.C. Chan, D. Yang and B.Y. Wu, J. Alloys Compd. 468 (2009) 553–557.
[15] Y. Yang, J. N. Balaraju and Z. Chen, in Proceedings of the 12th Electronics Packaging Technology Conference, Singapore, (2010) 801-806.
[16] L. Z. Song, Y. N. Wang, W. Z. Lin and Q. Liu, Surf. Coat. Technol. 202 (2008) 5146–5150.
[17] A.K. Gain, Y.C. Chan and K.C. Yung, Microelectronic Reliab. 51 (2011) 975–984.
[18] G. Dietz and H.D. Schneider, J. Phys.:Condens. Matter. 2 (1990) 2169-2178.

[19] B. Li, Y. Shi, Y. Lei, F. Guo, Z. Xia and B. Zong. J. Electron. Mater. 34 (2005) 217–224.
[20] S. Chada, W. Laub, R.A. Fournelle and D. S. Guan, J. Electron. Mater. 28 (1999) 1194-1202.
[21] Y.D. Lu, X.Q. He, Y.F. En, X. Wang and Z.Q. Zhuang, Acta. Mater. 57 (2009) 2560–2566.
[22] M.He, Z. Chen and G.J. Qi, Acta. Mater. 52 (2004) 2047–2056.
[23] C.B. Lee, J.W. Yoon, S.J. Suh, S.B. Jung, C.W. Yang, C.C. Shur and Y.E. Shin, J. Mater. Sci. -Mater. Electron. 14(2003) 487-493.
[24] P.L. Liu, J.K. Shang, Metall. Mater. Trans. A. 31 (2000) 2857-2866.
[25] K. Do, D. Lee, D.H. Ko, H. Sohn and M.H. Cho, Electrochem. Solid State Lett. 138 (2010) 284-286.
[26] S. Belyakov, H.V. Atkinson and S.P.A. Gill, J. Electron. Mater. 39 (2010) 1295–1297.
[27] Y. Yang, H. Lu, C. Yu and Y.Z. Li, Microelectronic Reliab. 51 (2011) 2314–2318.
[28] Y. Shi, J. Liu, Z. Xia, Y. Lei, F. Guo and X. Li, J. Mater. Sci. -Mater. Electron. 37 (2008) 507–514.
[29] Y.C. Sohn and J. Yu, J. Mater. Res. 20 (2005) 1931-1934.
[30] Z. Chen, M. He, A. Kumar and G.J. Qi, J. Electron. Mater. 36 (2007) 17-25.
[31] M.O. Alam, Y.C. Chan and K.C. Hung, Microelectronic Reliab. 42 (2002) 1065-1073.
[32] M.O. Alam, Y.C. Chan, and K.N. Tu, J. Appl. Phys. 94 (2003) 4108-4115.
[33] Y.C. Chan and D. Yang, Prog. Mater. Sci. 55 (2010) 428–475.

Figure captions

Fig.1 Reflow profile of the Sn-3.5Ag solder alloy.

Fig.2 Surface morphology and cross-section image of as-deposited (a, b) Ni–P layer and (c, d) Ni-P-TiO_2 layer

Fig.3 XRD patterns of Ni–P (upper) and Ni-P-TiO_2 (lower) coatings

Fig.4 AFM surface morphology of the (a) Ni-P and (b) Ni-P-TiO_2

Fig.5 Cross section view of reaction interfaces in as-reflowed (a) Sn-3.5Ag/Ni-P and (b) Sn-3.5Ag/Ni-P-TiO_2 joints

Fig.6 Cross section view of reaction interfaces in (a) Sn-3.5Ag/Ni-P and (b) Sn-3.5Ag/Ni-P-TiO_2 joints aged at 150 °C for 100 hours.

Fig.7 Cross section view of reaction interfaces in (a) Sn-3.5Ag/Ni-P and (b) Sn-3.5Ag/Ni-P-TiO_2 joints aged at 200 °C for 625 hours.

Fig.8 Thickness of the Ni_3Sn_4 layer in (a) Sn-3.5Ag/Ni-P and (b) Sn-3.5Ag/Ni-P-TiO_2 joints during aging at 150 ℃, 170 ℃ and 190 ℃ up to 625 h

Fig.9 Arrhenius plot of the growth of Ni_3Sn_4 layers in (a) Sn-3.5Ag/Ni-P and (b) Sn-3.5Ag/Ni-P-TiO_2 joints

Fig.10 Magnified view of reaction interfaces in Sn-3.5Ag/Ni-P-TiO_2 joints aged at 200 °C for 750 hours.

Fig.11 Schematic diagrams illustrating the diffusional formation mechanism at (a) Sn-3.5Ag/Ni-P and (b) Sn-3.5Ag/Ni-P-TiO_2 joints interface.

Fig.12 Ball shear strength result for Sn-3.5Ag/Ni-P and Sn-3.5Ag/Ni-P-TiO_2 joints.

Fig.13 SEM fracture surfaces of solder/Ni-P joint (a: aged for 400 hours and b: aged for 625 hours) and solder/Ni-P-TiO_2 solder(c and d, aged for 625 hours) joints after shear strength test.

Table captions

Table 1 Value of k determined from the slope of the linear regression

Figure.1
Click here to download high resolution image

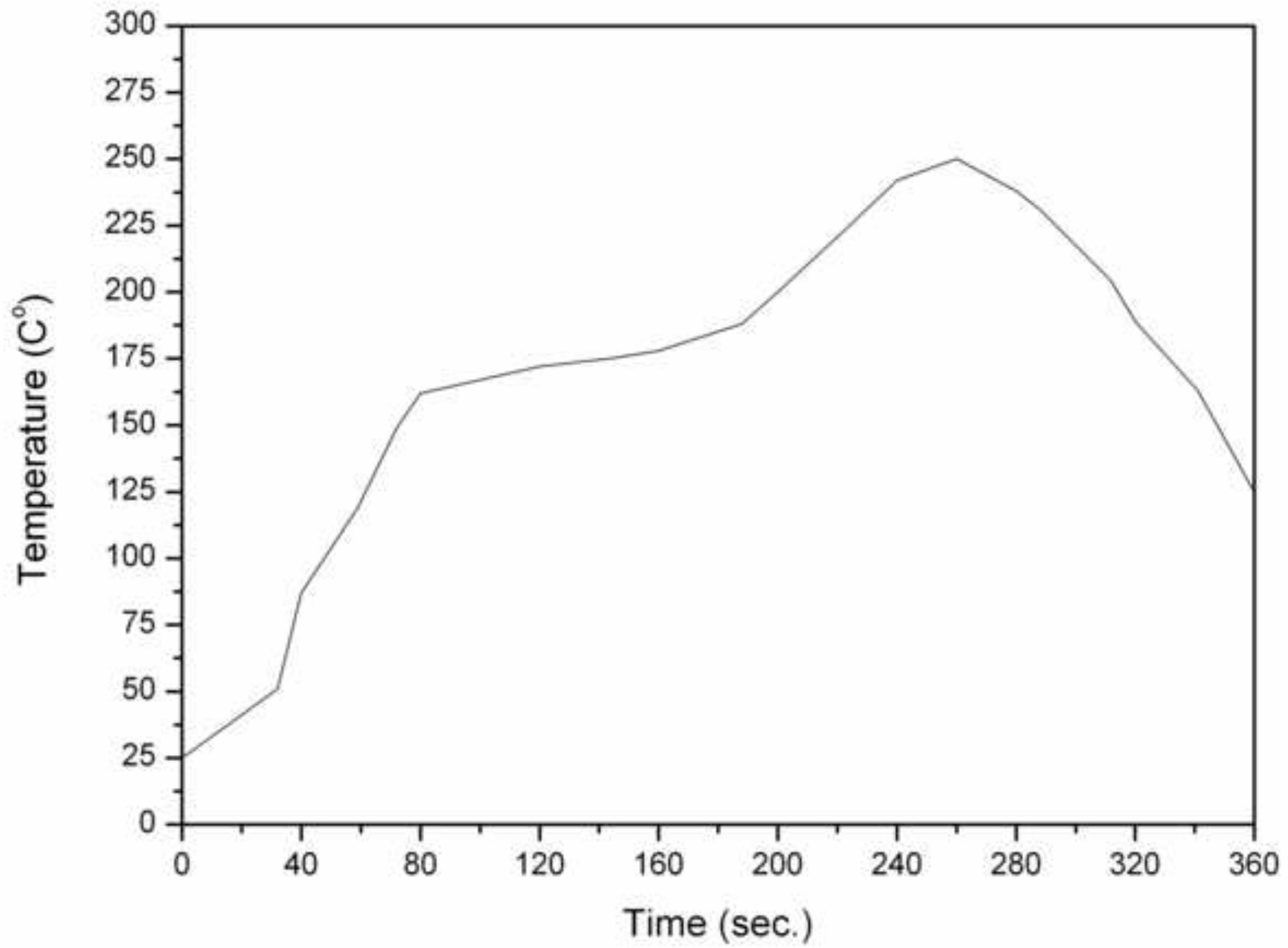

Figure.2

Click here to download high resolution image

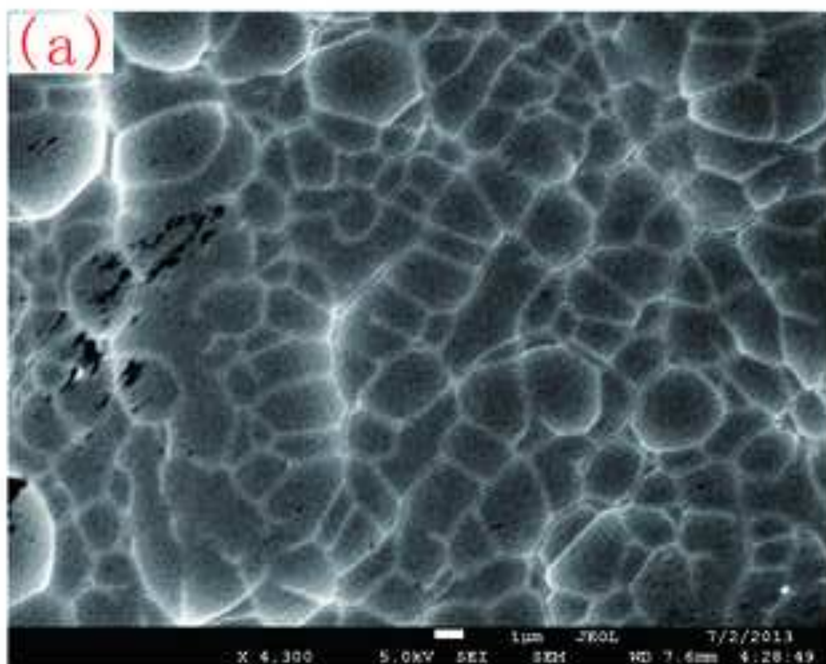

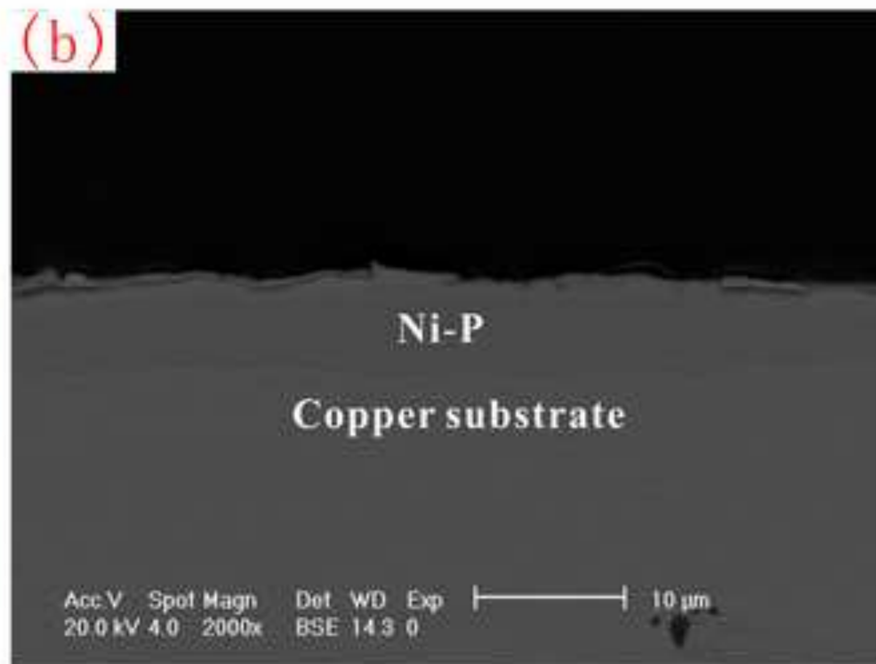

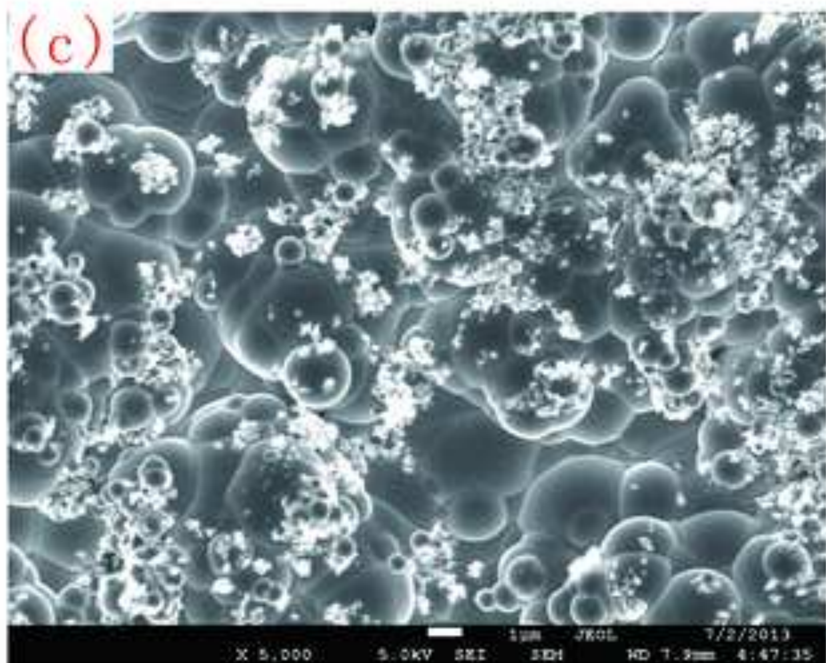

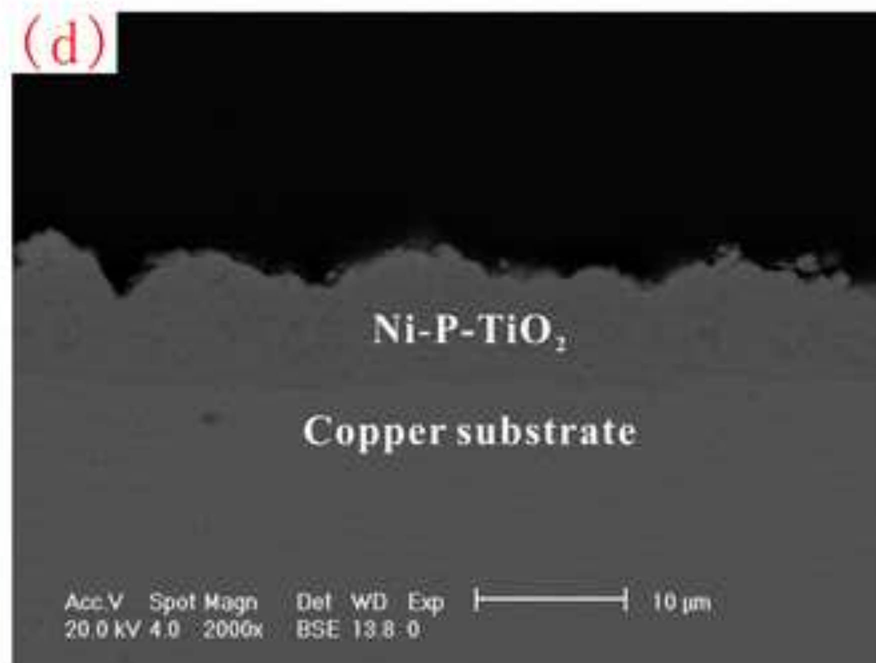

Figure.3

Click here to download high resolution image

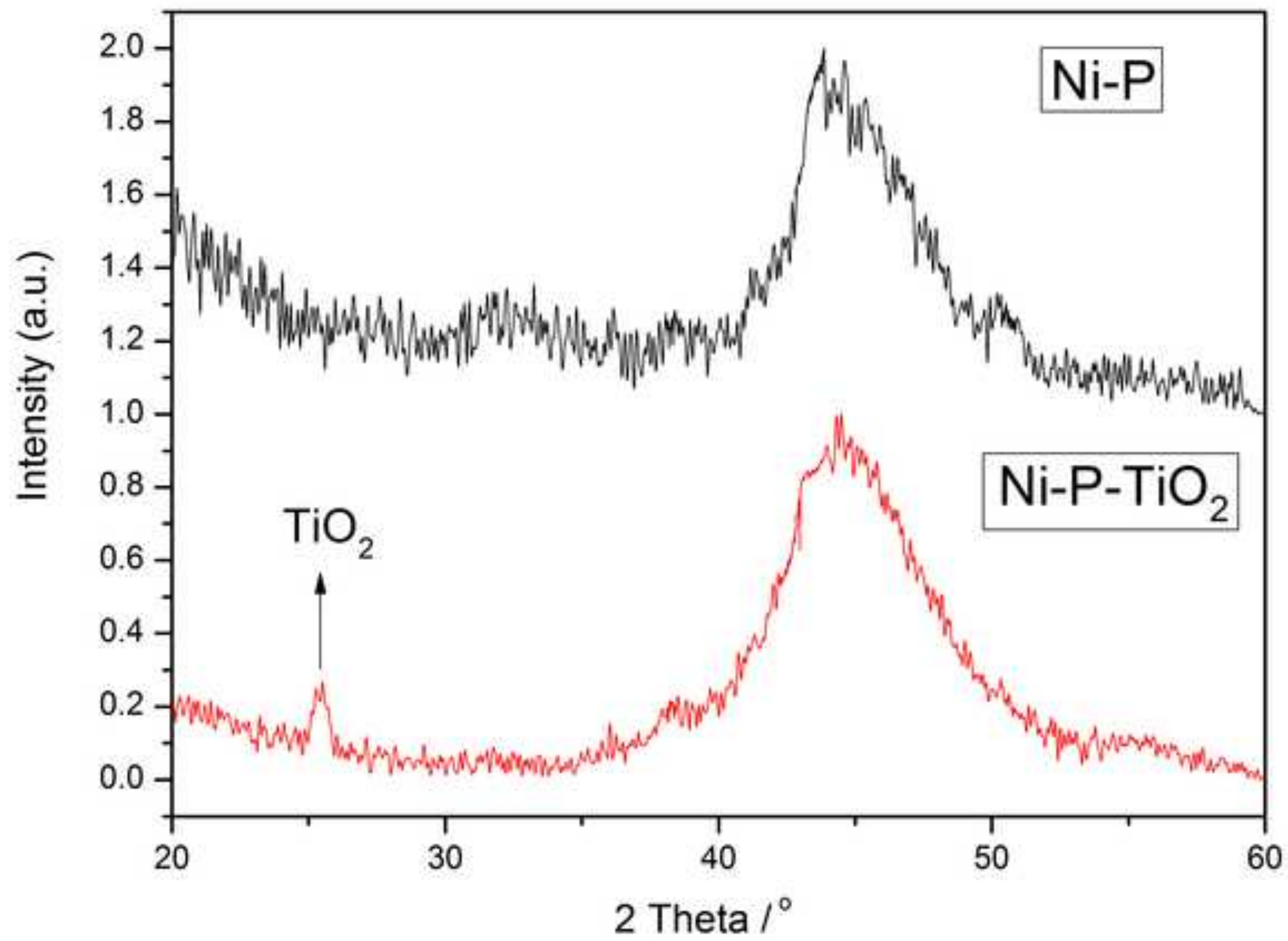

Figure.4
Click here to download high resolution image

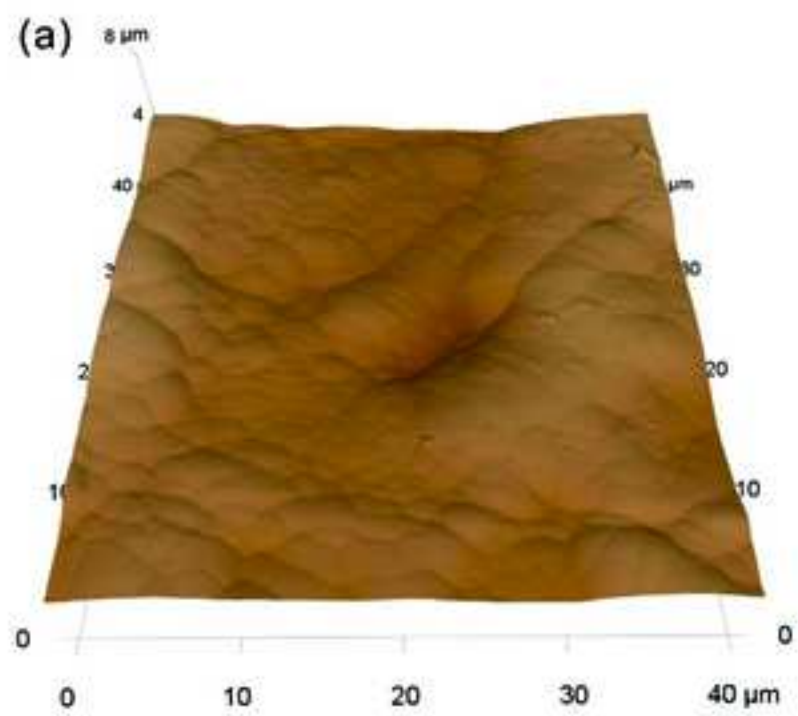

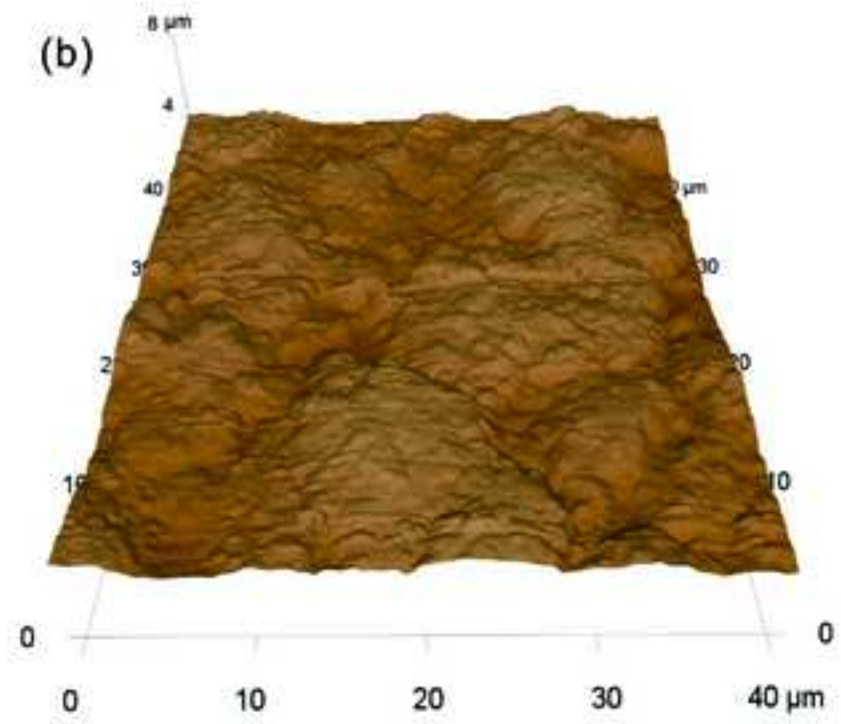

Figure.5
Click here to download high resolution image

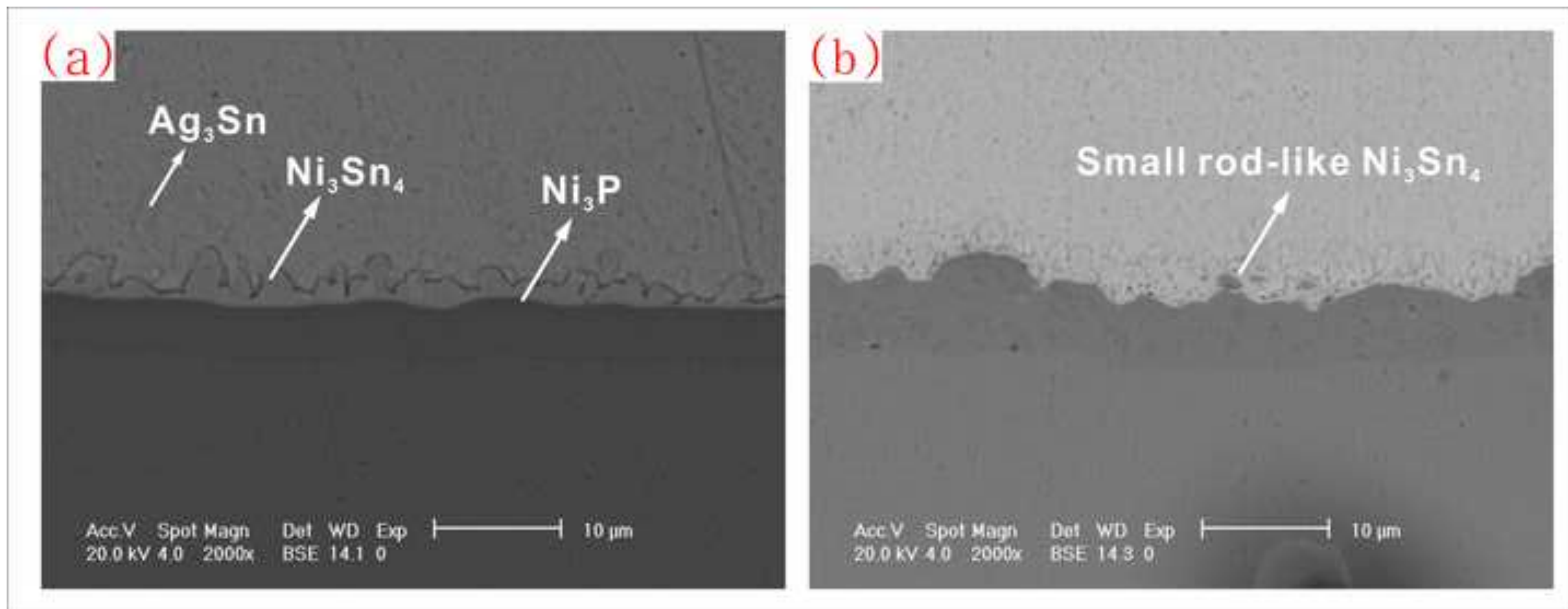

Figure.6

Click here to download high resolution image

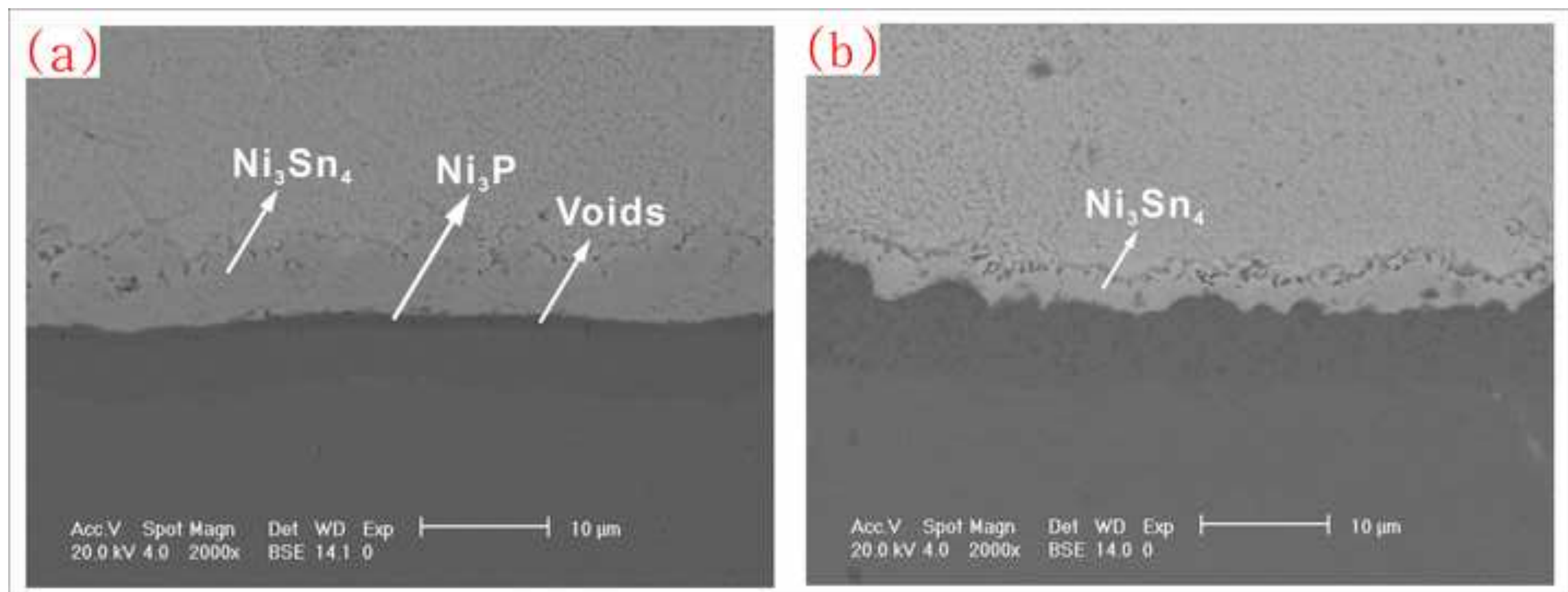

Figure.7
Click here to download high resolution image

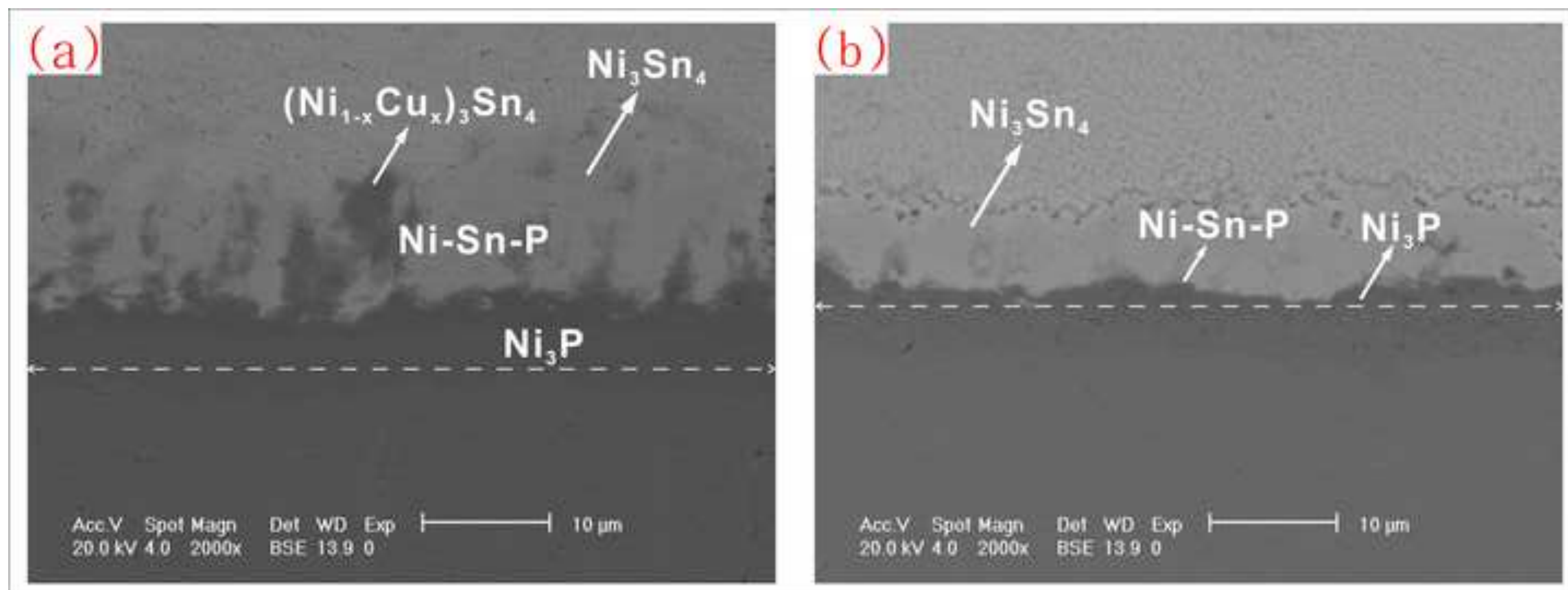

Figure.8
Click here to download high resolution image

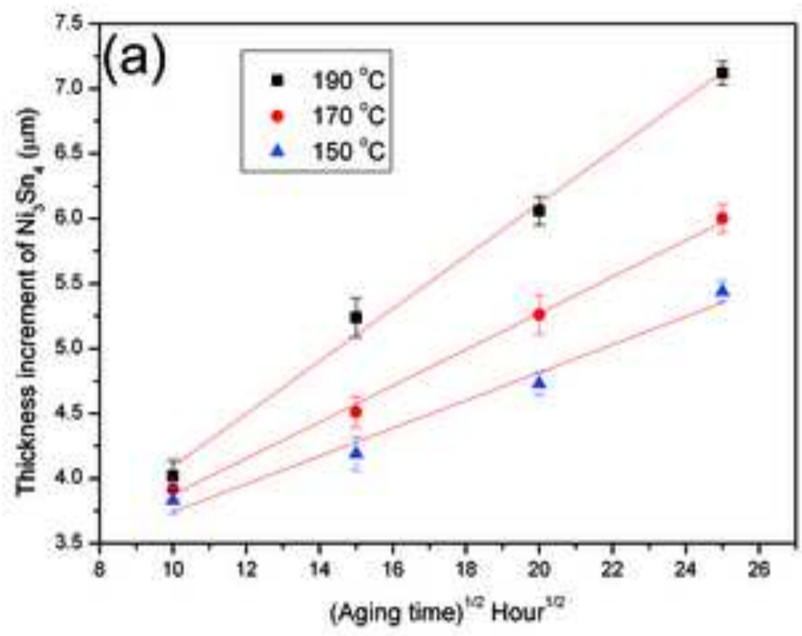

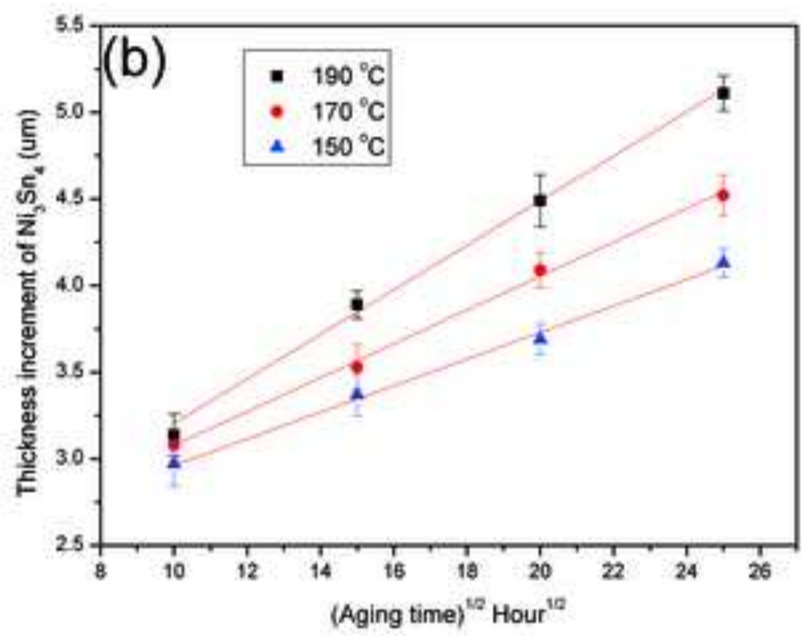

Figure.9
Click here to download high resolution image

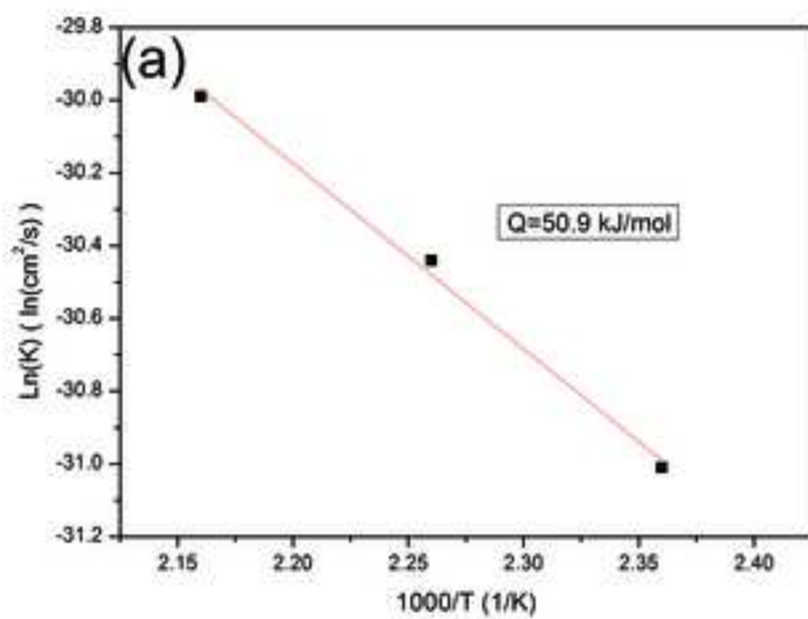

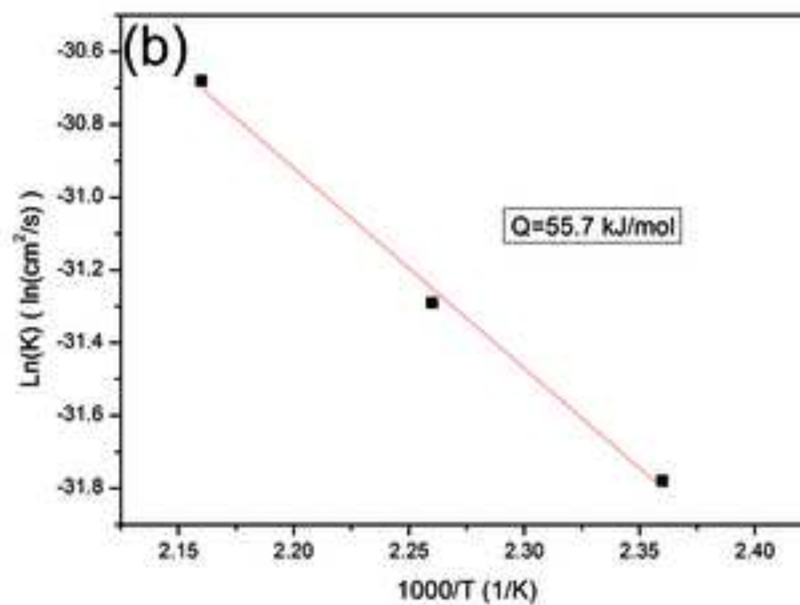

Figure.10
Click here to download high resolution image

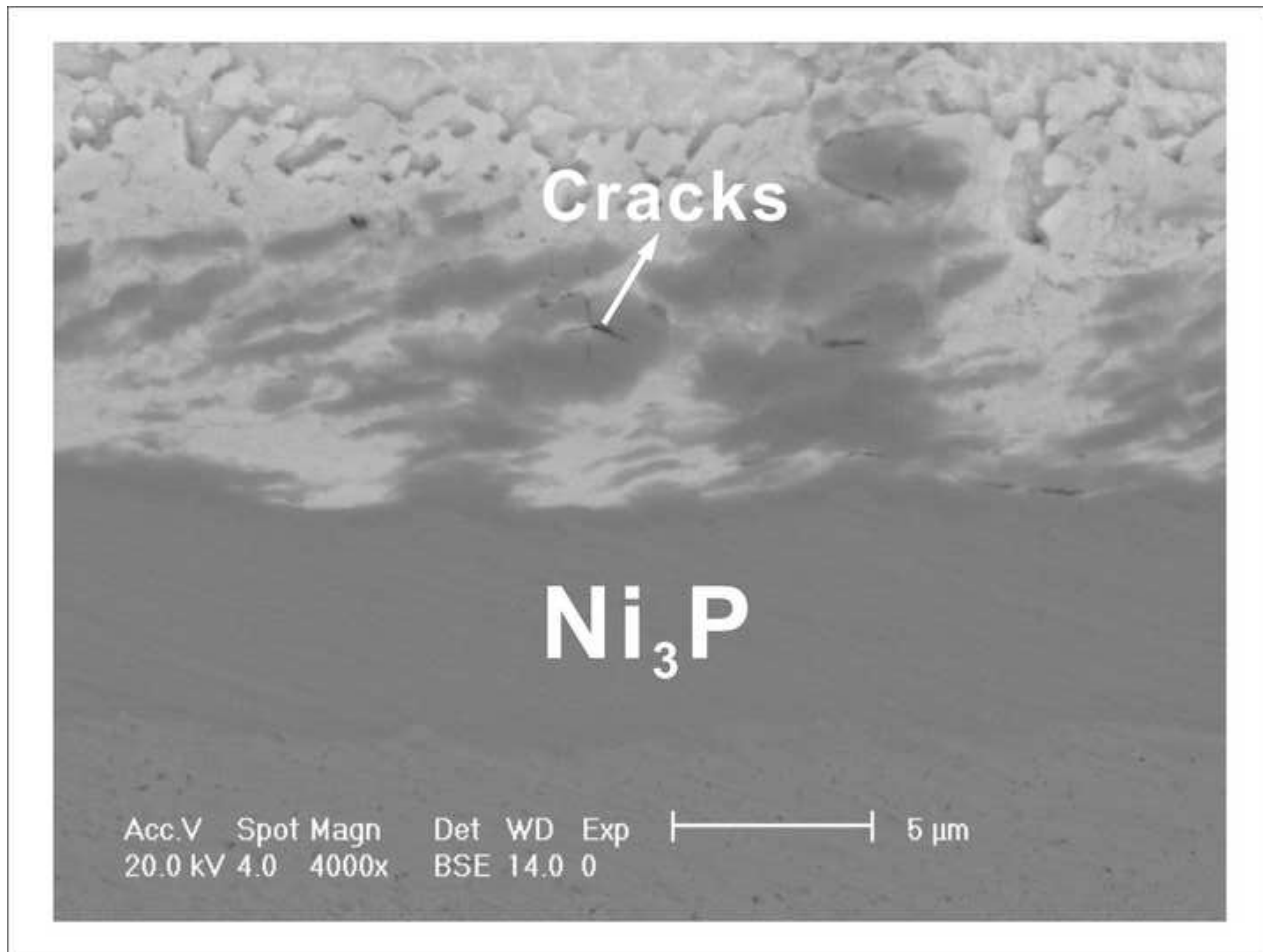

Figure.11
Click here to download high resolution image

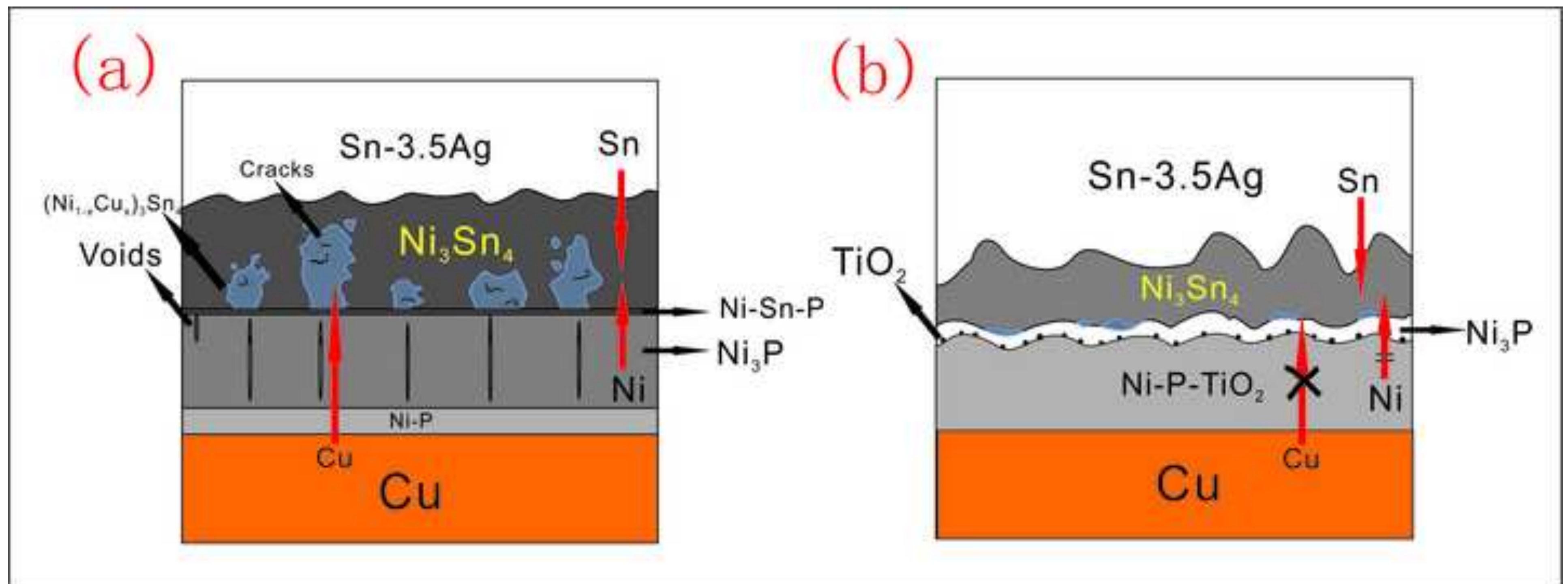

Figure.12
Click here to download high resolution image

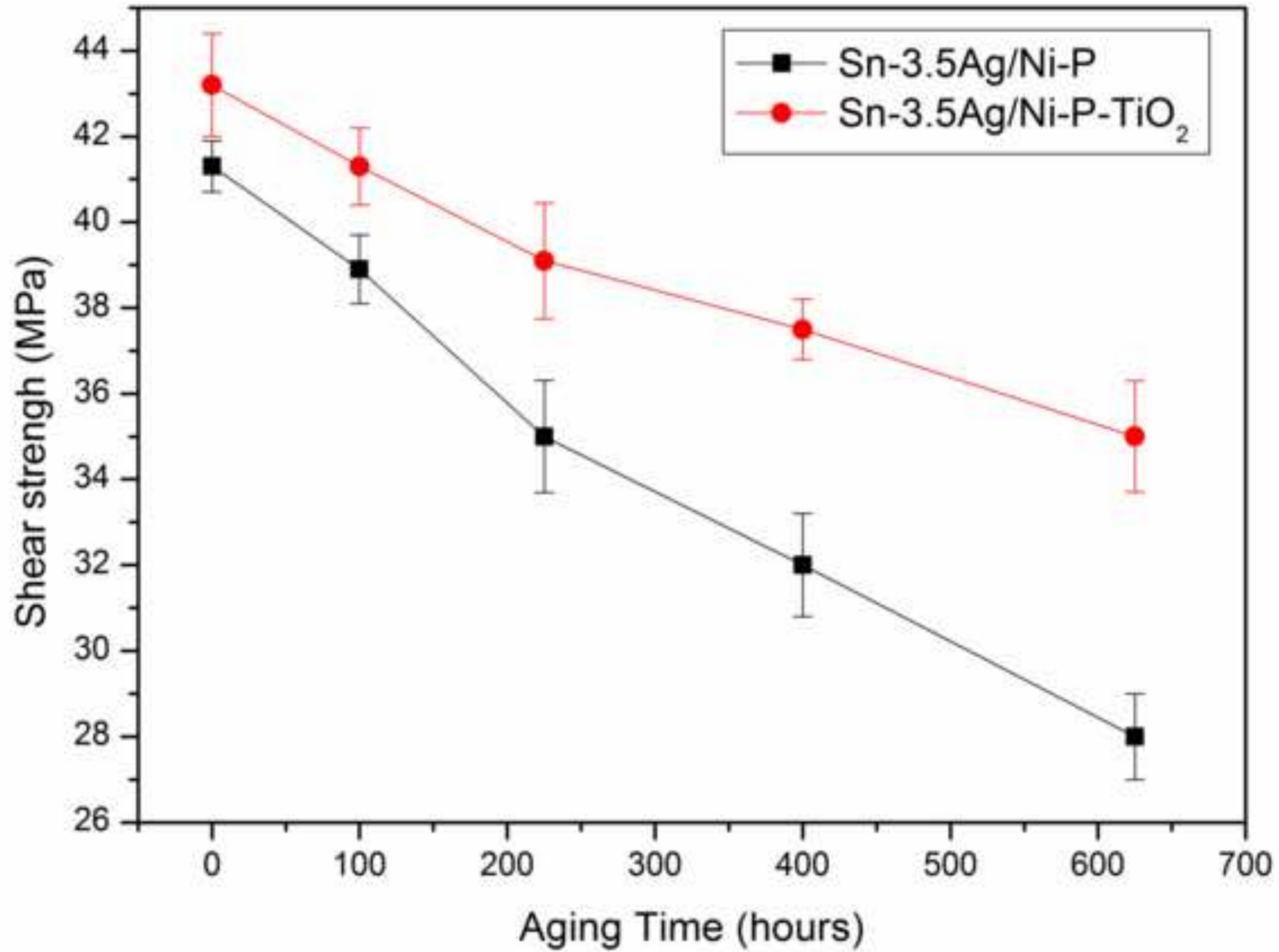

Figure.13

Click here to download high resolution image

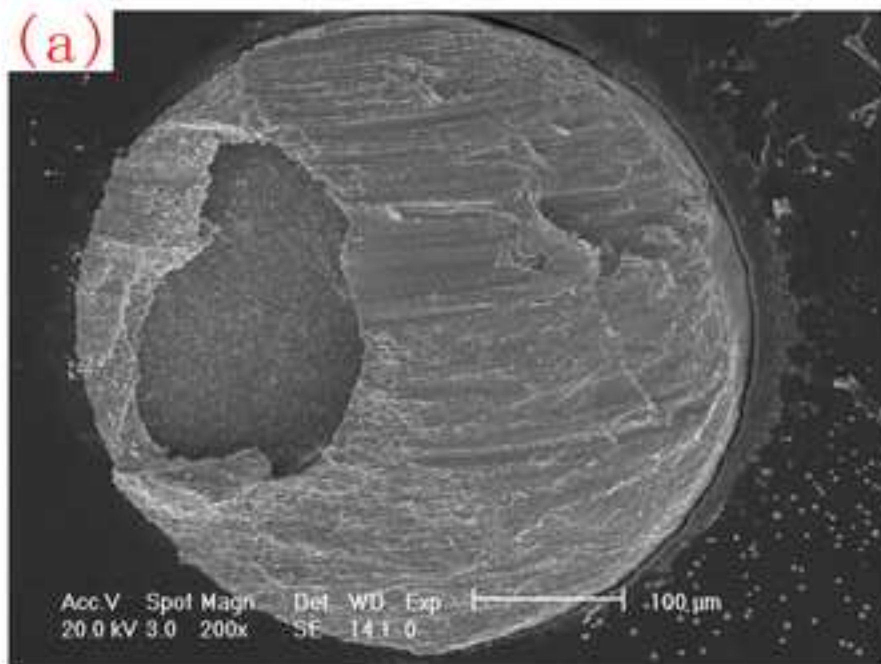

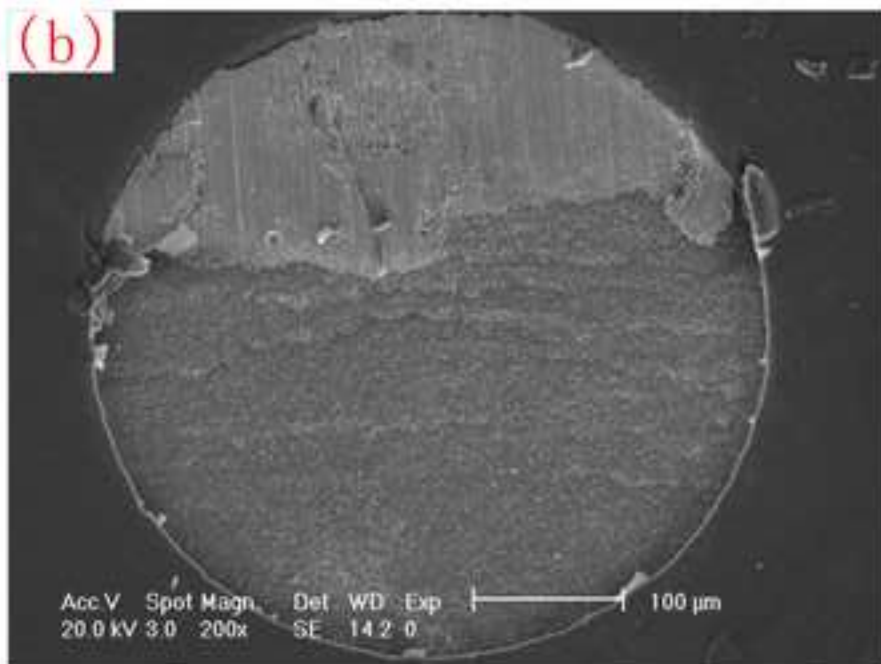

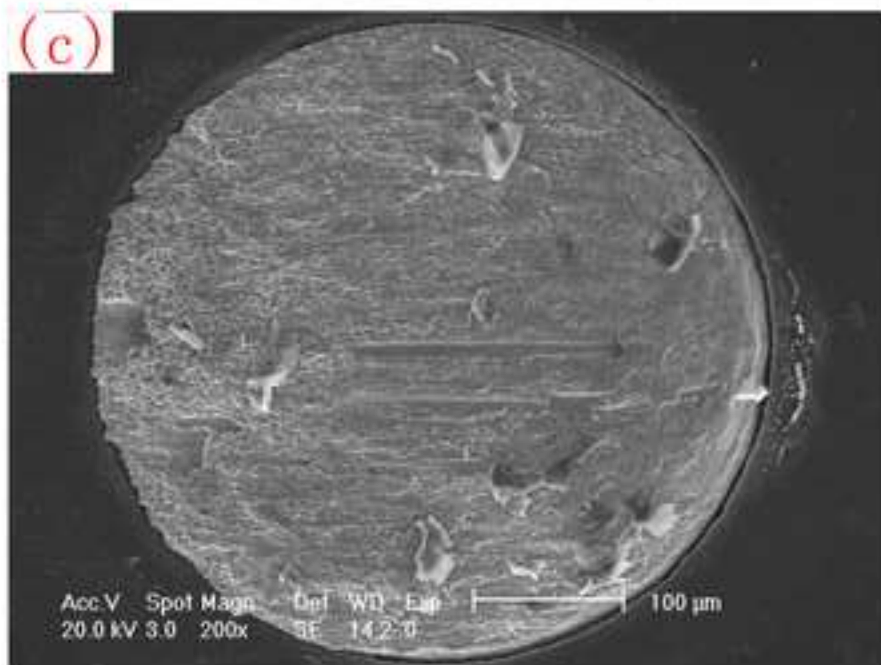

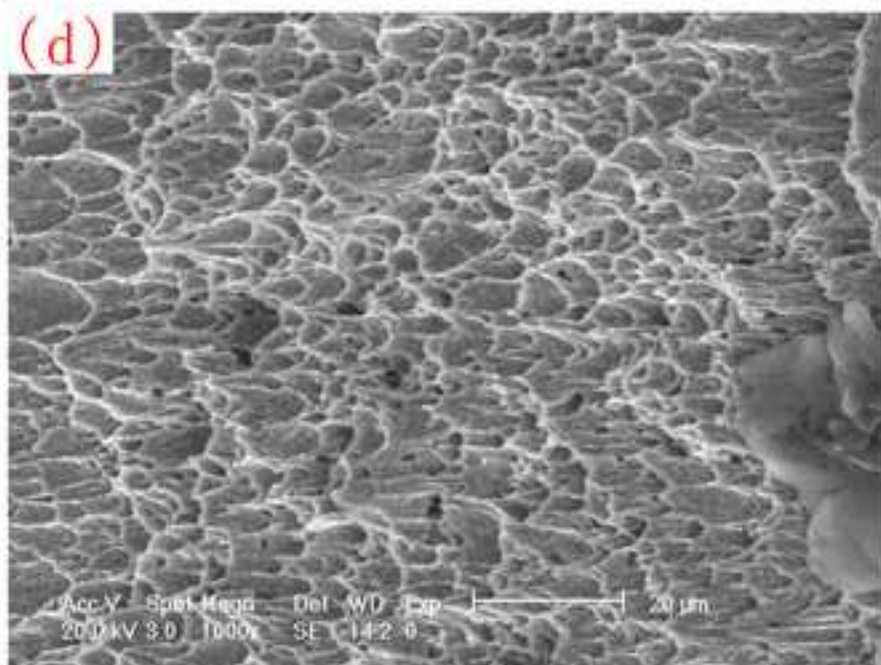

Table(s)

Table 1 Value of k determined from the slope of the linear regression

Temperature(℃)	solder/Ni-P		solder/Ni-P-TiO_2	
	$k^{1/2}$(μm/$s^{1/2}$)	k(cm^2/s)	$k^{1/2}$(μm/$s^{1/2}$)	k(cm^2/s)
150	1.81×10^{-7}	3.28×10^{-14}	1.26×10^{-7}	1.59×10^{-14}
170	2.39×10^{-7}	5.71×10^{-14}	1.63×10^{-7}	2.66×10^{-14}
190	3.02×10^{-7}	9.11×10^{-14}	2.17×10^{-7}	4.71×10^{-14}